Biodistribution studies of protein cage nanoparticles demonstrate broad tissue distribution and rapid clearance in vivo

Coleen R Kaiser[1]
Michelle L Flenniken[2,3]
Eric Gillitzer[3,4]
Ann L Harmsen[1]
Allen G Harmsen[1]
Mark A Jutila[1]
Trevor Douglas[3,5]
Mark J Young[3,4]

[1]Department of Veterinary Molecular Biology; [2]Department of Microbiology; [3]Center for Bio-Inspired Nanomaterials; [4]Department of Plant Sciences; and [5]Department of Chemistry and Biochemistry, Montana State University, Bozeman, Montana, USA

Abstract: Protein cage nanoparticles have the potential to serve as multifunctional cell targeted, imaging and therapeutic platforms for broad applications in medicine. However, before they find applications in medicine, their biocompatibility in vivo needs to be demonstrated. We provide here baseline biodistribution information of two different spherical protein cage nanoplatforms, the 28 nm viral Cowpea chlorotic mottle virus (CCMV) and the 12 nm heat shock protein (Hsp) cage. In naïve and immunized mice both nanoplatforms show similar broad distribution and movement throughout most tissues and organs, rapid excretion, the absence of long term persistence within mice tissue and organs, and no overt toxicity after a single injection. These results suggest that protein cage based nanoparticles may serve as safe, biocompatible, nanoplatforms for applications in medicine.

Keywords: protein cage nanoparticles, Cowpea chlorotic mottle virus, heat shock protein, biodistribution

Background

The use of nanoparticles in medicine holds the promise to provide dramatic improvements in diagnosis, imaging, and treatment of human disease and disorders (Brigger et al 2002; Emerich and Thanos 2003; Wickline and Lanza 2003; Allen and Cullis 2004; Service 2005a, 2005b). However, before this becomes a reality, there is a need for a thorough evaluation of nanoparticle toxicity and biodistribution in vivo. Although there are numerous reports promoting various nanoplatforms (5–100 nm) for medicine, few of them have been well characterized in vivo. Nanoparticles inherently have varying biological behaviors dependent on their size, shape, composition, surface chemistry, and associated physical properties. These attributes can greatly influence deposition, clearance from the body, and the toxicological nature of the nanoparticle (Powers et al 2006). There is a growing concern among scientists and the general public about the potential toxicity and biocompatibility of nanoplatforms (Nel et al 2006). At this time, a high priority must be placed on a more complete understanding of the circulation, clearance rates, blood half-life, stability, immunogenicity and organ biodistribution of nanoparticle delivery vehicles with the main goal of improving the functionality of nanoparticles in the biological environment so as to fully realize their biomedical value (Kayser et al 2005; Moghimi et al 2005).

Naturally occurring and synthetic nanometer scaled structures have the potential to be utilized as tissue and organ targeted cell-specific imaging and therapeutic delivery systems. There are a diversity of nanometer scale platforms being developed for such biomedical applications including: liposomes (Lee and Low 1995; Muller et al 2001; Barratt 2003), micelles (Roy et al 2003), polyamidoamine (PAMAM) dendrimer clusters (Choi et al 2005; Gurdag et al 2006), poly (D, L-lactic-co-glycolic acid) [PLGA] nanoparticles

Correspondence: Mark Young
Department of Plant Sciences and Plant Pathology, Ag BioScience Bldg. Rm #307, Bozeman, MT 59717, USA
Tel +1 406 994 5158
Fax +1 406 994 7600
Email myoung@montana.edu

(Yoo et al 1999, 2000), hydrogel dextran nanoparticles (Jana et al 2002; Na and Bae 2002), polysaccharide nanoparticles (Janes et al 2001), polyalkylcyanoacrylate nanocapsules (Damge et al 1988), lipid nanoparticles (Fundaro et al 2000), metal nanoshells (Loo et al 2004, 2005), amphiphilic core-shell nanoparticles (Sun et al 2005), viruses (Douglas and Young 1998; Flenniken 2004; Singh et al 2006) and other protein cage-based nanostructures (Hooker et al 2004).

The most extensively investigated nanoplatforms in terms of their in vivo biodistribution and toxicity are the nano materials commonly referred to as quantum dots (QDs) (Hardman 2006). Quantum dots are semiconductor nanocrystals (~2–100 nm) with distinctive optical and electrical characteristics (Bruchez et al 1998). Structurally, QDs consist of a metalloid crystalline core and a "cap" or "shell" that shields the core and renders the QD bioavailable. The QDs are "functionalized," or given secondary coatings, which improves water solubility, QD core durability, and assigns a desired bioactivity such as cell targeting. While more detailed studies remain to be performed, past studies have suggested a high degree of variability in QD biodistribution and toxicity in animal model systems that is likely dependent on multiple factors. These factors may include inherent physicochemical properties and environmental conditions including QD size, charge, concentration, outer coating bioactivity (capping material and functional groups), and oxidative, photolytic, and mechanical stability. This variability has suggested to some that under certain conditions QDs may pose environmental and human health risks (Hardman 2006). There is clearly a need to investigate the biodistribution of additional nanostuctures in order to expand our understanding of the compatibility of nanoparticles for application in medicine.

Viruses, virus-like particles (VLPs), and other protein cage nano architectures provide alternative platforms for combined cell-targeted imaging and therapeutic delivery systems. Protein cage systems that are currently being developed for biomedical applications share the common property of being assembled from a limited number of subunits to form a closed structure that defines an interior environment capable of housing therapeutic or imaging agents and an exterior surface capable of multivalent presentation of cell targeting ligands. Examples of spherical viruses, VLPs, and cellular protein cage architectures being explored for biomedical applications include the Cowpea chlorotic mottle virus (CCMV) (Speir et al 1995; Gillitzer et al 2002, 2006; Brumfield et al 2004), Cowpea mosaic virus (CPMV) (Brennan et al 2001; Chatterji et al 2002; Raja et al 2003; Blum et al 2004; Rae et al 2005; Lewis et al 2006), ferritins (Allen et al 2002), Dps-like protein cages (Wiedenheft et al 2005; Ramsay et al 2006) and small heat shock protein cages (Flenniken et al 2003, 2005, 2006; Kim et al 1998a, 1998b). Qualitative biodistribution studies with fluorescently labeled CPMV in mice and chick embryos indicate distribution of the particles in various tissues (ie, spleen, kidney, liver, lung, stomach, small intestine, lymph nodes, bone marrow, vascular endothelium and brain) after intravenous administration (Rae et al 2005; Lewis et al 2006). However, a quantitative study of protein-based nanoparticles has not been reported.

We present here quantitative bio-distribution and immunogenicity of two nanometer scale protein cage architectures; specifically, the plant virus based CCMV (Speir et al 1995; Gillitzer et al 2002; Brumfield et al 2004) and a small heat shock protein (Hsp) architecture originally isolated from the hyperthermophilic archaeon *Methanococcus jannaschii* (Kim et al 1998a). These two nanometer scale protein cage architectures have been genetically and chemically modified toward their development as potential cell targeted therapeutic and imaging agent delivery systems (Gillitzer et al 2002, 2006; Flenniken et al 2003, 2005; Allen et al 2005). Cowpea chlorotic mottle virus is a member of the *Bromoviridae* family (Francki 1985). Its capsid is composed of 180 copies of the coat protein which can self- assemble without packaging its viral genome to form an icosahedral particle with an exterior diameter of 28 nm and an interior diameter of 24 nm (Brumfield et al 2004). Genetic and chemical modification of CCMV has been used to impart cell targeting and imaging capacity to the protein cage architecture (Gillitzer et al 2002, 2006). The Hsp assembles into an empty 24 subunit cage with octahedral symmetry that has an exterior diameter of 12 nm and an interior diameter of 6.5 nm (Kim et al 1998a, 1998b). The overall structure of Hsp resembles a multi-windowed hollow sphere. The Hsp cages have been derivatized with therapeutic molecules and a genetic variant, HspG41C-RGD4C, has been shown to bind melanoma cells in vitro (Flenniken et al 2003, 2005, 2006). We report the in vivo biodistribution and clearance of non-targeted CCMV and the Hsp protein cages in both naïve and immunized mice.

Methods

Purification and characterization of HspG41C

Cloning, mutagenesis, and purification of the heat shock protein (Hsp) cage from an *E. coli* heterologous expression

system was previously described (Flenniken et al 2003). The HspG41C cages, with interior exposed thiols, were characterized by size exclusion chromatography (Superose-6, Amersham-Pharmacia), dynamic light scattering (DLS) 90 plus (Brookhaven Instruments), and by transmission electron microscopy (TEM) (LEO 912 AB) (Supplemental Figure 1).

Purification and characterization of CCMV S102C and CCMV K42R

Two genetic variants of CCMV were utilized for these experiments, CCMV S102C for epifluorescence studies and CCMV K42R for biodistribution studies. Purification of CCMV S102C from the *Pichia pastoris* (yeast) heterologous expression system was performed as previously described (Speir et al 1993; Brumfield et al 2004). The primer sequences utilized for PCR mediated mutagenesis of CCMV S102C were: S102C for 5′ gttgcttcccagtgtttgtggtaccgtgaaatcctgtg 3′ and S102C rev 5′ cacaggatttcacggtaccacaaacactgggaagcaac 3′. The integrity of the entire CCMV S102C coding sequence was confirmed by sequencing on an ABI 310 automated capillary sequencer using Big Dye chain termination sequence technology (Applied Bio Systems, Foster City, CA, USA). The CCMV S102C capsids were purified and characterized by size exclusion chromatography (Superose 6, Amersham-Pharmacia), dynamic light scattering (DLS) 90 plus (Brookhaven Instruments), and transmission electron microscopy (TEM) (LEO 912 AB) (Supplemental Figure 1). CCMV K42R capsids were characterized (Fox et al 1996) and purified from plants as previously described (Bancroft and Hiebert 1967).

Derivatization of CCMV S102C and HspG41C with Texas Red®C_2-maleimide (Invitrogen)

Cysteine containing genetic variants, CCMV S102C and HspG41C, were chemically derivatized with Texas Red®C_2-maleimide (Invitrogen) using methods described in (Gillitzer et al 2002; Flenniken et al 2003). The cages (100 mM HEPES 50 mM NaCl pH 6.5) were reacted with Texas Red®C_2-maleimide (Invitrogen) in a concentration of 3-fold molar excess per subunit. The reactions proceeded for 30 minutes at room temperature followed by overnight incubation at 4 °C. Texas-Red® labeled cages were purified from free dye by size exclusion chromatography (Superose 6, Amersham-Pharmacia) in Dulbecco's phosphate buffered saline pH 7.4.

Iodination of protein cages (CCMV K42R and HspG41C)

Protein cages were iodinated utilizing IODO-BEADS Iodination Reagent (Pierce) according to manufacturer's instructions. Unincorporated ^{125}I were removed with desalting columns (Zeba Desalt Spin Columns, Pierce): two rounds of desalting were performed. The iodinated protein cages was characterized by absorbance spectroscopy, size exclusion chromatography (Superose 6, Amersham Pharmacia), dynamic light scattering (Brookhaven 90Plus), and transmission electron microscopy (TEM) (Leo 912 AB) (Supplemental Figure 1). The specific activity of ^{125}I labeled protein cages was determined from counts associated with the sample compared to a linear regression fit to the counts from ^{125}I standards (ranging from 0–1000 nCi) (x-axis) plotted with their corresponding counts per minute (y-axis) (Beckman Gamma 4000 Counting System). Typically, specific activity for Hsp cage samples was ~20 nCi/μg and ~250 nCi/μg for CCMV samples. The incorporation of ^{125}I, in terms of specific activity (nCi/μg), was about 10-fold greater in CCMV K42R as compared to HspG41C cages. This discrepancy is most likely because CCMV has more surface accessible tyrosines (5 per subunit; 900 per cage; exterior Tyr 50, 157, 159, 190, interior Tyr 138) than Hsp (2 per subunit; 48 per cage; interior Tyr 96, subunit interface Tyr 106).

In vivo biodistribution experiments with ^{125}I-HspG41C or ^{125}I-CCMV nanoparticles

Mice received an intravenous dose, via the tail vein, of either 50 μg of ^{125}I-HspG41C or ^{125}I-CCMV cage in a 200 μL volume. The dose of radiation ranged from approximately 0.3 to 0.5 μCi of cage. The nanocages were allowed to circulate for 1 to 24 hours before animals were sacrificed with a lethal dose of sodium pentobarbital. When a lack of pedal response was apparent mice were opened and the abdominal aorta clipped. A 70 μL blood sample was obtained and all organs excised and weighed separately. The blood, tissue and injected dose samples were then transferred into vials and counted on a Beckman Gamma 4000 Counting System.

Calculations of radioactivity in blood and organ samples

Tissue radioactivity measures were in counts-per-minute (cpm) and background adjusted. The percent of recovered dose per gram of tissue or per organ was calculated as follows:

$$\%\ \text{of injected dose/g of tissue} = \frac{\text{Activity recovered/g of tissue}}{\text{Administered dose radioactivity}} \times 100$$

$$\%\ \text{of injected dose/organ} = \frac{\text{Activity recovered/organ}}{\text{Administered dose radioactivity}} \times 100$$

In order to compare the burden of deposition in various organs the percent of injected dose per gram of tissue was used. However, some tissues weigh less than 1 gram and result in percentages greater than 100. The percent injected dose/organs, urine and feces samples were totaled for mice at 1 and 24 hours so as to determine the total percent of dose recovered in each experiment.

Animals

The experimental animal protocol used for all studies including the ^{125}I trials was approved by the Institutional Animal Care and Use Committee and the Safety and Risk Management Office at Montana State University. Female BALB/c mice, 10–14 weeks old, weighing on average 18–22 gm each, were purchased from Charles River Laboratories (Wilmington, MA). The 24 hour mice were housed in Nalgene® Metabolic Cage for Single Mouse (Rochester, NY) under normal conditions with *ad libitum* access to finely ground sterilized rodent chow and water.

Immunizations

Female BALB/c mice were immunized with either a 50 μg HspG41C or CCMV protein dose intravenously injected into the tail vein. Mice received the dose in a 200 μL volume at week 1 and two weeks later (week 3). At week 4 a blood sample was obtained to confirm immunization and then week 5 mice received an IV challenge of 50 μg of ^{125}I-labeled cage to determine particle biodistribution as stated below.

SDS-polyacrylamide gel electrophoresis

Samples were run using SDS-Polyacrylamide Gel Electrophoresis (PAGE) under denaturing conditions with TR-CCMV S102C and TR-HspG41C controls. Gels were visualized first by fluorescence (inverted image; Molecular Imager FX, BioRad) and then by Coomassie Brilliant Blue staining and compared to molecular weight markers.

Vibratome sections and fluorescent microscopy

Mouse lungs were instilled with 3% low melt agarose (kept at 37 °C) and allowed to set-up in cold PBS for later sectioning. One-hundred micron thick agarose lung sections were cut on a Leica VT1000S vibrating-blade microtome (Leica Microsystems Nussloch GmbH, Germany). Fresh kidney and liver cuts (100 microns thick) were also made using the vibrating microtome; these tissues samples were not agarose filled. Tissue sections were wet mounted on slides, cover slipped and viewed with the Nikon Eclipse E800 microscope (Nikon, Inc., Melville, NY) and imaged using the Nikon Digital Camera DXM1200 and MetaVue software (Molecular Devices Corporation, Downingtown, PA).

Hematoxylin and eosin staining

A morphological examination of lung, liver, spleen and kidney was conducted with tissues obtained from mice sensitized and challenged with either of HspG41C or CCMV cage protein. The organs were excised from mice at 1 and 24 hrs after the challenge and fixed in 10% phosphate-buffered formalin (Fisher Scientific), dehydrated in a graded series of ethanol, embedded in paraffin, and cut into 5 micron thick serial sections. Sections were then stained using hematoxylin and eosin (H and E), and the morphology of the various tissues examined using the Nikon Eclipse E800 microscope and images taken with the Nikon Digital Camera DXM1200 and MetaVue software as stated above.

Measurement of IgG and IgE cage specific antibodies

Total IgG specific HspG41C and CCMV in sera was measured by direct enzyme-linked immunosorbent assay (ELISA). The sera were kept frozen at –80 °C before analysis. Each well of a 96-well polystyrene plate was coated with 50 μL of either a CCMV or Hsp solution at a protein concentration of 0.5–1.0 μg/mL and incubated overnight at 4 °C. The plate was then washed four times with a 2% horse serum solution prior to each well being blocked with 100 μL of a non-specific binding site blocking buffer (1% bovine serum albumin in PBS) and again incubated for two hours at room temperature. The plate was washed once more with the 2% horse serum solution and 100 μL of serum diluted in blocking buffer was added and the plate incubated for 2 hours at room temperature. The plate received four additional washes and 100 μL per well of goat anti-mouse peroxidase conjugated IgG, diluted in blocking buffer to a 1:500 concentration, was added then incubated for one hour at room temperature. The samples were again washed four times and ABTS substrate added, allowed to react for 15 minutes and visualized at 415 nm on a microplate reader (VERSA$_{MAX}$ Microplate Reader, Molecular Devices, Sunnyvale, CA, USA).

Sera cage specific IgE was also measured by an ELISA assay. An affinity purified anti-mouse IgE capture mAb (2 μg/mL; clone R35-72, BD Bioscience, San Diego, CA, USA) was used to coat a 96-well ELISA plate (flat-bottom, high-binding, polystyrene; Costar, Corning, NY, USA) at 4 °C overnight. Next, the plates were washed three times with PBS/Tween 20 and incubated with a non-specific binding site blocking buffer (1% bovine serum albumin in PBS) for 1 h at room temperature. After incubation, the plates were again washed three times with PBS/Tween 20 and serum samples, controls, and standards applied; 1 hr incubation at 37 °C followed. Again the plates were washed three times and 100 μL per well of biotinylated anti-mouse IgE (2 μg/mL; clone R35-118, BD Biosciences) was added and the plate incubated for 1 h at room temperature. After washing, 100 μL per well of horseradish peroxidase avidin D (0.5 μg/mL; Vector Laboratories, Inc, Burlingame, CA) was added and the plate incubated at 37 °C for 30 minutes. The plates were washed with PBS/Tween 20 five last times. The presence of bound Ab was detected by the addition of 100 μL per well of *o*-phenylenediamine dihydrochloride (SIGMAFAST™ OPD, Sigma-Aldrich Co., St. Louis, MO) and visualized at 405 nm on a microplate reader ($VERSA_{MAX}$ Microplate Reader, Molecular Devices, Sunnyvale, CA). The Ig contents of the serum samples were compared with standard curves generated from the 405 nm absorbance levels of known amounts of IgG or IgE.

Statistical analysis

The majority of the data were analyzed using GraphPad PRISM (version 4.00; 2003). Data are presented as mean values ± standard deviation (SD) and the unpaired Student *t*-test with calculations of a two-tailed p-value were utilized to determine significance; differences with a p-value < 0.05 were considered significant. Results from the ^{125}I-CCMV, ^{125}I-HspG41C, and free ^{125}I experiments were evaluated by GraphPad PRISM one-way ANOVA to determine statistical significance; differences between the free ^{125}I and ^{125}I-labeled cage were evaluated using the Bonferroni's Multiple Comparison Test for multiple post-hoc comparisons. The comparisons of percent injected dose/organ for selected organs from the ^{125}I-CCMV and ^{125}I -HspG41C experiments were made using two-way ANOVA analysis with the GLM procedure of SAS (version 8.2; Statistical Analytical Systems Institute, Inc., Cary, NC, USA). The main effects of immune status (naïve vs. immunized) and time (1 hr vs 24 hr), and the interaction between immune status and time were evaluated. When the interaction was not significant the main effect means are reported. If the interaction was significant, then the interaction mean was reported. If the treatment F-test was significant ($p < 0.05$) the treatment least square means were separated by the LSD method.

Results

In vivo localization of Texas Red-labeled CCMV and HspG41C by fluorescence microscopy

Genetic variants of both CCMV (CCMV S102C) and Hsp (Hsp G41C) were chemically derivatized with Texas Red®(TR) in order to visualize the cages by epi-flourescence microscopy. Texas Red-labeled CCMV and TR-HspG41C cages were intravenously (IV) injected into mice from which various tissues were subsequently harvested and evaluated. Fluorescent images from vibratome sections of tissues demonstrated TR-HspG41C cages in the lung, liver and kidney and TR-CCMV in the liver and kidney at 1 hour post IV injection (Figures 1 and 2). Neither the TR-HspG41C nor TR-CCMV particles appear to be associated with any one cell type in the lung; rather, they were visible on pulmonary endothelial surfaces, interstitial perivascular areas, and in alveolar lymphatic ducts (Figure 1). The TR-HspG41C introduced into the mouse intranasally (IN) appeared rapidly in the lymph nodes of the respiratory tract (tracheobronchial and cervical lymph nodes) within 1 hour post instillation (data not shown). The TR-labeled protein cages appeared to freely move in and out among the epithelial cells of the airways, the pulmonary endothelial cells, and pulmonary draining lymph nodes.

TR-labeled cages were also evident in the sinusoids of the mouse liver at 1 hour after IV injection (Figures 1 and 2). They appeared to be associated with either phagocytic Kupffer cells or endothelial cells of the sinusoid radiating from the terminal hepatic venule, but were otherwise evenly dispersed throughout the liver. This association of the cages with these cell types was not surprising, as both have the capacity to interact with particulate materials via phagocytosis, thus protecting the systemic circulation by clearing the plasma of foreign material (Steffan et al 1986; Dini et al 1995).

As seen in lung and liver, both cage types were present in the kidney. One hour after IV injection, cages could be seen in the convoluted tubules and interlobular connective tissue of the mouse kidney. By 24 hours post injection cages were still visible primarily in the convoluted tubules of the kidney (Figure 1), although with less intensity than seen at 1 hour, and in the cortical lymphatics. In summary, these

results indicate that both non-cell targeted CCMV and Hsp protein cages can be rapidly found within the lungs, kidneys and liver, declining by 24 hours post IV injection.

In vivo biodistribution studies of ^{125}I labeled cage

In order to evaluate the biodistribution of CCMV and Hsp cages they were radiolabeled with ^{125}I. Both the CCMV and Hsp protein cages were rapidly and broadly distributed to a majority of the mouse tissue and organ types. Within 1 hr post injection, both the CCMV and Hsp protein cages were detected in all examined tissues and organs, with 0.1% or less of the injected dose in the brain (Table 1). The biodistribution of ^{125}I-HspG41C or ^{125}I-CCMV cages in naïve mice at the 1 hour time point did not significantly differ from one another in terms of percent injected dose/gram of tissue (%ID/g), with the exception of the salivary gland (Figure 3). The salivary gland of mice injected with ^{125}I-HspG41C had 56% greater %ID/g of tissue than the ^{125}I-CCMV injected mice. The five sites of greatest deposition for the ^{125}I-HspG41C or ^{125}I-CCMV cages at 1 hour were the bladder, thyroid, liver, spleen, and salivary gland. Thus, independent of protein cage size or amino acid composition, a similar pattern of rapid biodistribution of both protein cage types to most tissue and organ types was observed.

The biodistribution of ^{125}I-labeled cage was evaluated in naïve and immunized mice. Overall, by 24 hours post injection, both the CCMV and Hsp protein cages had been significantly cleared to a similar extent from most organs in naïve mice except the thyroid where levels actually increased over 24 hours (Figures 3 and 4; Tables 1 and 2). In general, greater than 80% of the recovered labeled protein cages had been removed by 24 hrs as compared to 1 hr post injection. Even though there was an overall reduction of both protein cages, there were significant differences ($p < 0.05$) in distribution of the two cage types in the liver, spleen and kidney, such that a greater %ID/g of liver, spleen and kidney was found in ^{125}I-CCMV versus ^{125}I-HspG41C injected mice. It was evident the majority of the ^{125}I-HspG41C or ^{125}I-CCMV cages protein cages were secreted through the urine and feces (56%–66% of dose) (Table 2). These results demonstrated that independent of protein cage type, size or amino acid composition, a similar pattern of rapid removal of both protein cages from most tissue and organ types in naive mice was observed.

The CCMV and the Hsp protein cages demonstrated similar biodistribution patterns in both naïve and immunized mice. Similar to the biodistribution patterns observed in naive mice, both the CCMV and the Hsp protein cages were detected in all tissue and organ types except the brain in immunized mice. When ^{125}I-HspG41C or ^{125}I-CCMV protein cages were administered IV to mice previously immunized with either the Hsp or CCMV protein cages, the distribution pattern at 1 hour was similar for both types of protein cages expressed as either a percentage of dose per gram of tissue or per organ basis (Figures 3 and 4; Tables 1 and 2). Two exceptions to this were the %ID of ^{125}I-CCMV found per gram of both lung and kidney of immunized mice differed significantly from the %ID of ^{125}I-HspG41C injected in those tissues ($p < 0.05$). In immunized mice at 1 hr, the %ID/gm of lung found in mice receiving iodinated HspG41C cage was 4.5 times greater than that in the lungs of mice receiving iodinated CCMV (30.8% ID/g versus 6.8% ID/g) (Table 2 and Figure 3). Conversely, a comparison of the %ID/g of kidney indicated a greater amount (1.4 times) of iodinated cage present in CCMV-immunized mice than in HspG41C-immunized mice at 1 hour.

When the biodistribution of labeled cages was examined on a per total organ basis, the pattern of deposition of the two types of nanocages among mice organs at 1 and 24 hours was similar ($p > 0.05$) (Figure 4). With regards to naïve versus immunized mice, the distribution of nanocages in the whole organs was similar with the exception of the liver and GI tract. At 1 hour, the ^{125}I-HspG41C IV administered naïve mice had approximately 2 times more of the injected dose in the GI tract than the Hsp-immunized mice, while the CCMV-naïve mice had 2.5 times more cage associated counts in the GI tract than CCMV-immunized mice. The opposite was true for the %ID in the liver; at 1 hour 2.8 times more of the ^{125}I-HspG41C dose and 1.6 times more of the ^{125}I-CCMV dose was found in the liver of immunized versus naïve mice. The %ID/g of thyroid was appreciably less at the 1 hour time point in immunized versus naïve mice for ^{125}I-HspG41C or ^{125}I-CCMV cage ($p < 0.05$; 3.5 and 22.3 times less respectively) (Figure 3).

In order to test the possibility of free ^{125}I release from the radiolabeled protein cages skewing the distribution, an investigation into the biodistribution of free ^{125}I in mice using identical methods to those used in the protein cage biodistribution was conducted. The biodistribution of free ^{125}I was notably different than the biodistribution of the injected iodinated protein nanocages. The results of the free ^{125}I study indicated that at 1 hour post injection the majority of free ^{125}I was found in the tegument (24.6 % ID) and gastrointestinal tract (16.44 %ID). The organs associated with the highest %ID/g of tissue were the thyroid and bladder (221.3% and 208.9%/g tissue respectively). Gamma counts obtained from

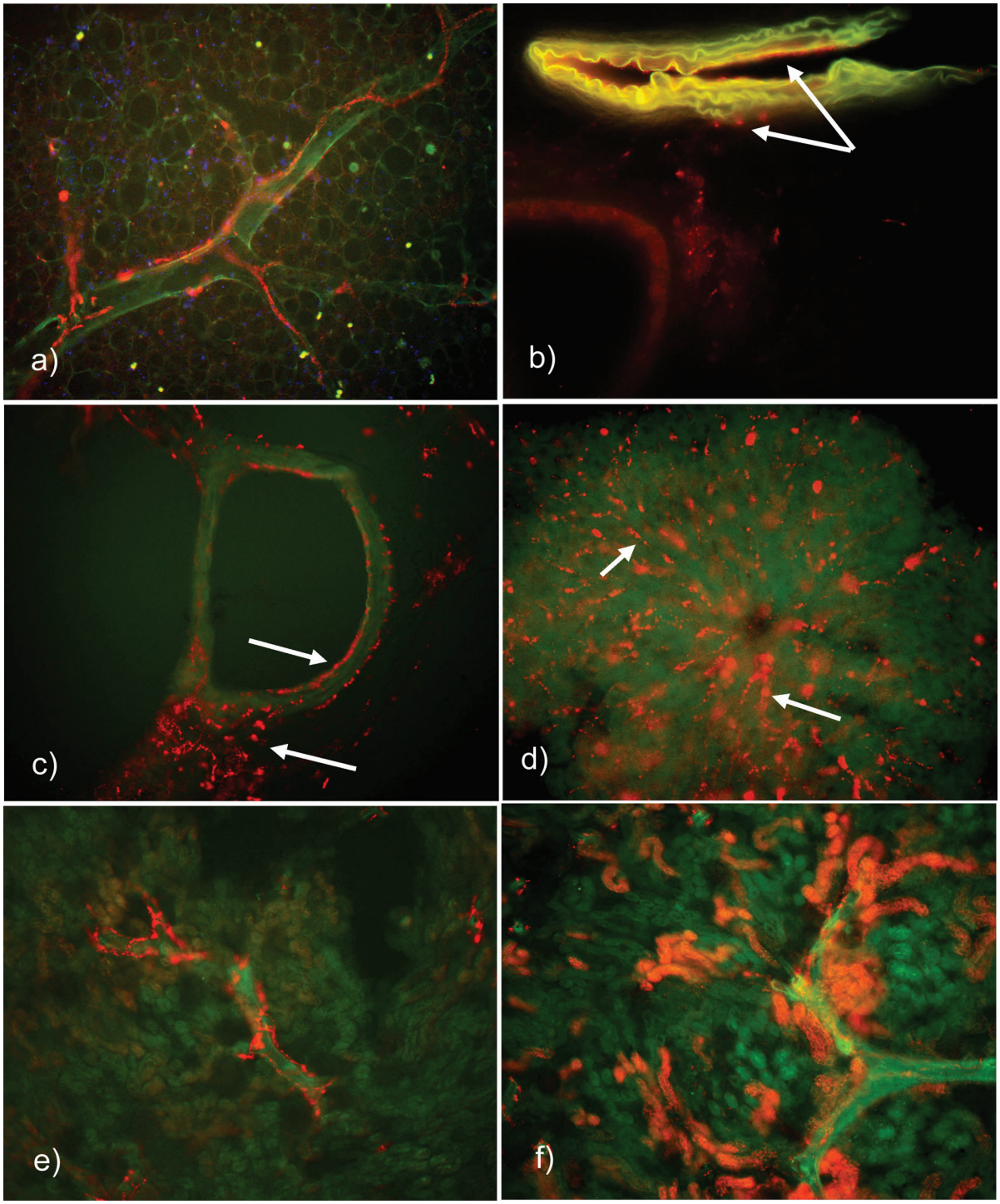

Figure 1 Epifluorescence microscopy images exhibiting Texas Red-Labeled HspG41C in various mouse tissue vibratome sections after IV instillation of 50–100 μg protein. (**a**) Lymphatic duct filled with particles surrounding an alveolar airway at 1 hour (200x original magnification). (**b**) Pulmonary arteriole at 1 hour post injection (50 μg Protein) with specific fluorescence visible on the endothelial surface and perivascular areas of the interstitium (note arrows). (**c**) Pulmonary airway at 1-hour – pointing to particles situated on the endothelial surface and intersititially (100x original magnification). (**d**) Hepatic lobule at 30 minutes after instillation – terminal hepatic venule with radiating sinusoids and HspG41C-Texas Red fluorescene most likely associated with Kupffer cells (note arrows; 200x original magnification). (**e**) Frontal sections of the kidney at 24 hours post injection – interlobular capillary and cortical lymphastics satiated with fluorescent labeled cage (100x original magnification). (**f**) Kidney frontal sections at 1 hour demonstrating fluorescence in the convoluted tubules and interlobular connective tissue (100x original magnification).

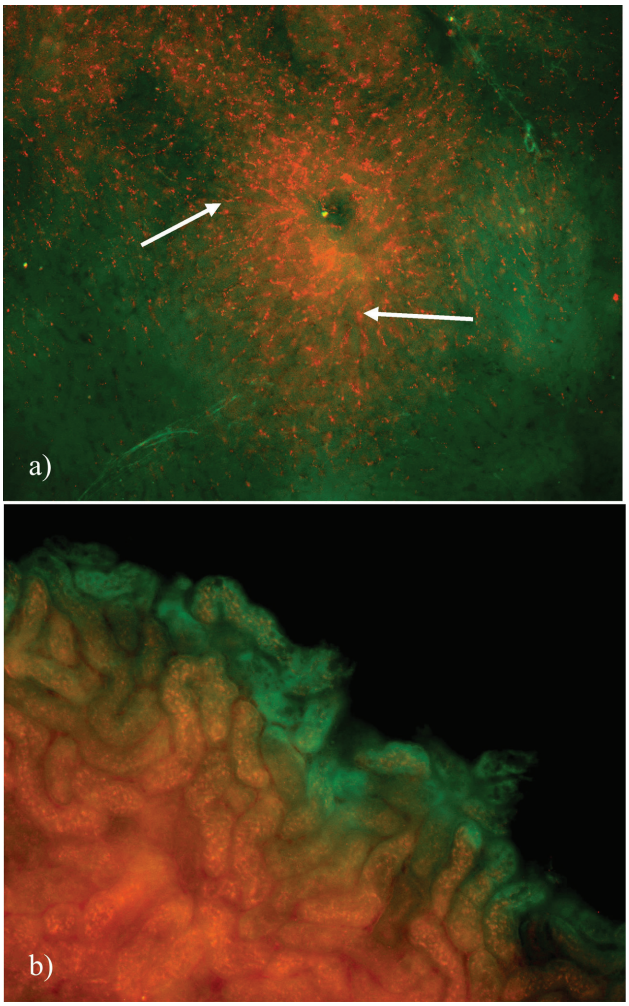

Figure 2 Fluorescence microscopy displaying Texas Red-labeled CCMV cage in mouse liver and kidney at 1 hour post IV instillation of 50μg protein. (**a**) Hepatic lobule with terminal hepatic venule and radiating sinusoids filled with CCMV Texas Red-labeled particles most likely associated with Kupffer cells (note arrows; 100x original magnification). (**b**) Kidney frontal sections at 1 hour exhibiting Texas Red labeled CCMV cage in the convoluted tubules (200x original magnification).

the 24 hour collection of urine were high as well (63.7%ID, 74.28% of dose recovered) (Figure 5). The presence of free ^{125}I- in the lungs of injected mice had less %ID/g of tissue than the ^{125}I-HspG41C-immunized injected mice at 1 hour (5.03% vs 30.78%; $p < 0.05$). The %ID/g of liver and spleen at 1 and 24 hours was significantly less ($p < 0.05$) in free ^{125}I-injected mice compared to mice injected with ^{125}I-labeled cage (Figure 5). One-way ANOVA analysis revealed a significant difference at the 1 and 24 hour time points ($p < 0.05$) when the distribution of ^{125}I-HspG41C or ^{125}I-CCMV in the thyroids of naïve and immunized mice were compared to free ^{125}I injected mice; immunized mice receiving iodinated HspG41C or CCMV had less %ID/g of thyroid than mice receiving free ^{125}I alone (Figure 5).

In general, the biodistribution of two different protein nanocages in the organs and tissues of naïve or immunized mice were similar, both at 1 and 24 hours post injection. As well, no real pattern of preferential accumulation in one tissue or organ type was readily apparent, with the possible exception of the thyroid and liver.

Excreted form of IV injected ^{125}I-labeled CCMV and Hsp protein nanocages in mouse urine

Both cage types (^{125}I-HspG41C and ^{125}I-CCMV) were nearly completely cleared from mouse tissues by 24 hours. The total percent of injected dose recovered in the urine alone ranged from 51% to 60%; from the feces and urine combined values were 56.6%–63.3%, while the total recovered dose ranged from 64% to 89% and none of these were significantly different.

Various analyses were conducted to determine the form of the excreted cage in the urine. In this regard, direct visualization of viral concentrates of urine samples (100,000 × g viral pellet fraction) by transmission electron microscopy failed to identify intact virus particles. In addition, enzyme-linked immunosorbent assay (ELISA) and western immunoblot analysis utilizing CCMV polyclonal antiserum failed to detect intact either 28 nm CCMV particles or intact coat protein subunits. No evidence was found that CCMV protein cages were secreted in the urine intact. Urine samples from mice IV injected with TR-HspG41C or TR-CCMV were analyzed using a SDS-polyacrylamide gel electrophoresis; first imaged with fluorescence and subsequently stained with Coomassie Blue. Results, when compared to control urine spiked with TR-HspG41C or TR-CCMV, indicated that the cages were not intact and coat protein subunits were not detected (data not shown). These observations suggest that in the ^{125}I-HspG41C or ^{125}I-CCMV injected mice the cages were degraded *in vivo* and excreted in components smaller than the cage protein subunits.

Immune and hypersensitivity response

An ELISA was used to analyze serum from immunized mice for either HspG41C- or CCMV-specific IgG. Serum samples were obtained from mice seven days after receiving two 50 μg IV injections two weeks apart. Results indicated animals were highly positive for cage protein-specific IgG (data not shown). These mice were then used in the ^{125}I-labeled cage biodistribution experiments described above. The CCMV-immunized mice, and to a lesser extent HspG41C-immunized mice, exhibited signs of distress 5–7 minutes post injection of

Table 1 CCMV and Hsp protein cage distribution in mouse tissues at 1 and 24 hours after IV injection

Tissue type	CCMV 1 hr		CCMV 24 hr		CCMV (I) 1 hr		CCMV (I) 24 hr		Hsp 1 hr		Hsp 24 hr		Hsp (I) 1 hr		Hsp (I) 24 hr	
	%ID	%ID/g	%ID	%ID/g	%ID	%ID/g	%ID	%ID/g	%ID	%ID/g	%ID	%ID/g	%ID	%ID/g	%ID	%ID/g
Thyroid	2.97	192.99	9.40	126.42	0.67	8.66	7.97	81.61	2.49	132.64	6.75	483.0	0.97	37.52	4.89	76.39
Bladder	9.04	120.02	0.10	0.38	1.54	21.58	0.15	0.82	4.19	176.45	0.08	1.41	1.40	59.34	0.27	1.79
Liver	20.61	22.79	4.82	5.07	33.80	36.81	3.90	3.94	14.89	20.56	0.50	0.59	42.11	45.73	1.11	1.05
Spleen	1.36	14.50	0.31	2.45	1.31	10.11	0.26	1.49	1.43	15.02	0.05	1.12	1.40	13.95	0.16	0.99
Salivary gland	1.40	12.36	0.05	0.28	2.21	11.88	0.02	0.12	2.22	22.04	0.01	0.14	1.61	16.89	0.03	0.17
Kidney	2.72	9.61	0.46	1.44	1.93	6.21	0.14	0.43	1.81	7.34	0.06	0.19	0.52	4.43	0.57	1.79
Lungs	0.85	4.76	0.08	0.37	1.36	6.82	0.03	0.15	0.76	5.09	0.02	0.13	3.26	30.78	0.05	0.24
Heart	0.44	4.54	0.02	0.15	0.44	2.12	0.01	0.04	0.35	3.19	0.03	0.07	0.27	2.09	0.01	0.05
GI Tract	16.57	6.83	0.54	0.21	6.77	3.10	0.27	0.11	16.79	8.32	0.20	0.09	7.84	3.90	0.35	0.13
Tail	2.44	4.28	0.46	0.72	3.95	7.28	0.86	1.53	4.23	7.81	0.35	0.71	1.62	3.42	1.01	1.98
Blood	6.31	6.10	0.22	0.18	5.63	5.51	0.08	0.08	10.28	9.52	0.09	0.09	4.21	4.10	0.12	0.11
Tegument	12.57	3.45	0.74	0.20	13.38	3.62	0.68	0.20	17.58	4.91	0.32	0.10	11.38	3.07	0.78	0.20
Head	3.34	3.02	0.14	0.13	3.89	3.44	0.07	0.07	5.03	4.30	0.06	0.05	2.77	2.56	0.75	1.47
Repro tract	1.58	2.65	0.05	0.08	1.03	1.65	0.03	0.05	1.72	4.70	0.04	0.04	1.45	2.22	0.04	0.07
Upper quad	4.83	1.62	0.33	0.10	7.77	2.34	0.32	0.11	6.69	2.06	0.20	0.07	4.47	1.53	0.29	0.10
Lower quad	6.73	1.44	0.43	0.15	8.24	1.96	0.38	0.10	8.97	2.04	0.17	0.05	6.78	1.48	0.55	0.12
TBLN	0.01	0.38	0.00	0.00	0.02	0.25	0.00	0.00	0.03	1.17	0.01	0.16	0.01	0.40	0.00	0.00
Brain	0.11	0.30	0.01	0.01	0.11	0.25	0.00	0.00	0.15	0.41	0.01	0.01	0.09	0.23	0.00	0.00
Olfactory bulbs	0.02	0.21	0.00	0.00	0.00	0.05	0.00	0.00	0.02	0.44	0.01	0.03	0.01	0.45	0.00	0.00
Urine	-	-	55.97	-	-	-	53.39	-	-	-	57.48	-	-	-	50.72	-
Feces	-	-	7.36	-	-	-	5.88	-	-	-	5.65	-	-	-	5.91	-
Total	93.86	-	81.44	-	94.01	-	74.42	-	99.59	-	72.04	-	92.10	-	67.57	-

Abbreviations: %ID, Percent injected dose; %ID/g, Percent injected dose/gm of tissue; (I), Immunized mice.

HspG41C (n = 7 for naïve 24 hr mice; n = 8 for immunized mice; salivary gland, n = 4 for naïve 1 and 24 hr mice); CCMV K42R (n = 8).

(A)

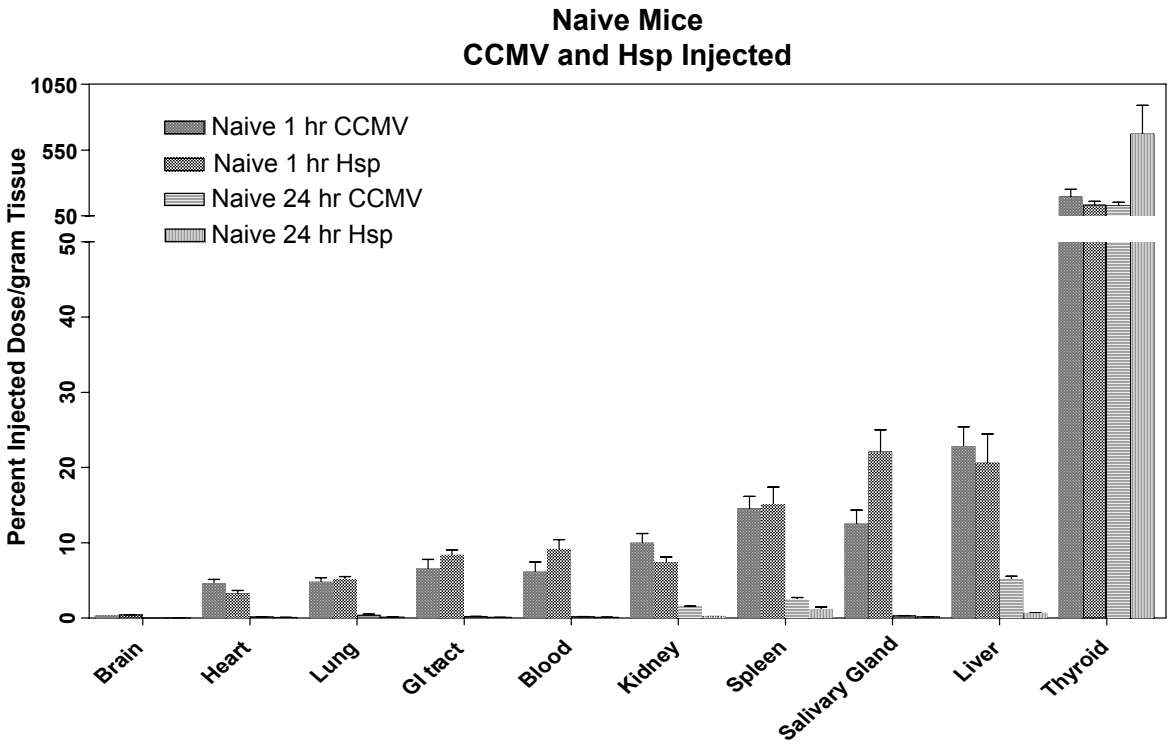

(B)

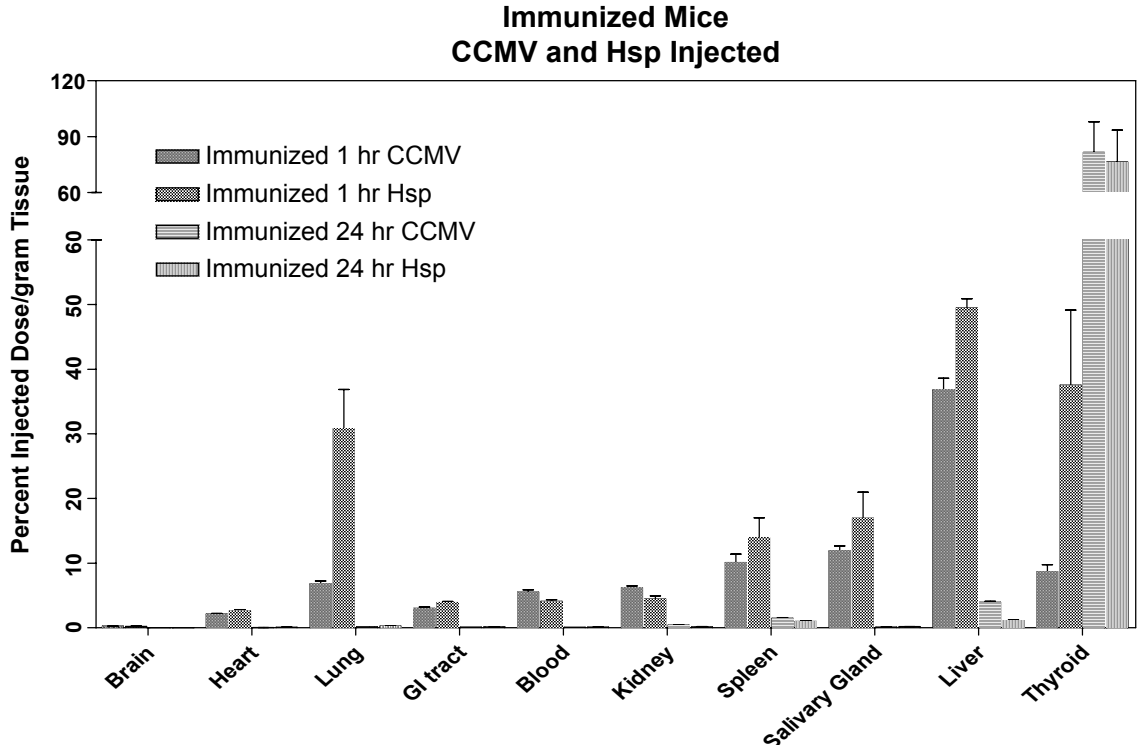

Figure 3 Selected organ distribution of ^{125}I-labeled cages on a percent injected dose/gm of tissue basis. (**A**) Naïve mice receiving 50 μg protein IV injection of either ^{125}I-HspG41C or ^{125}I-CCMV cage at 1 and 24 hours. (**B**) Immunized mice receiving 50 μg protein IV injection of either ^{125}I-HspG41C or ^{125}I-CCMV cage at 1 and 24 hours.

(A)

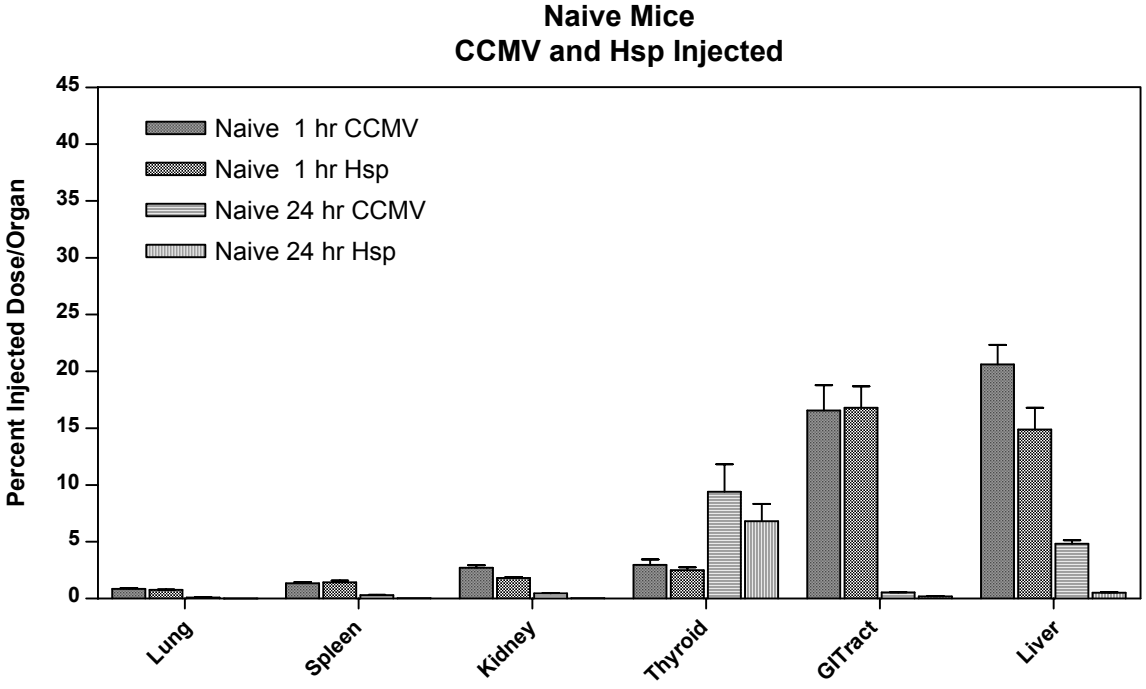

(B)

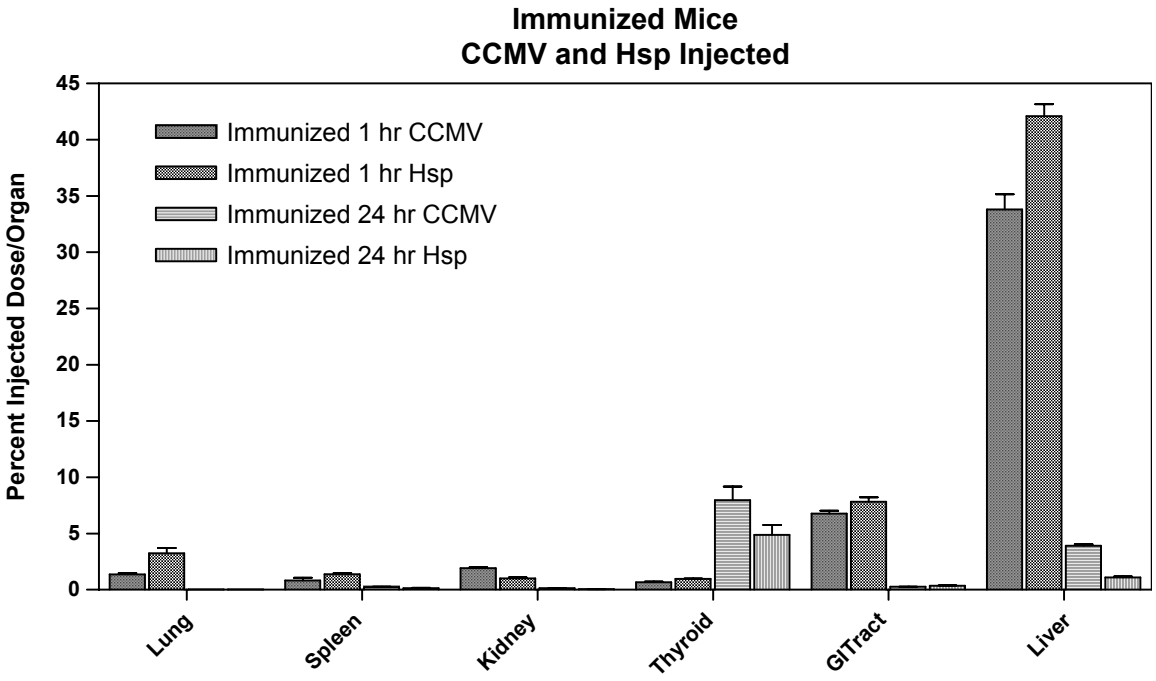

Figure 4 Percentage of dose per organ in selected tissues. (**A**) ^{125}I-labeled CCMV and Hsp cage (50 μg protein) tail injected into naïve mice at 1 and 24 hours post injection (**B**) ^{125}I-labeled CCMV and Hsp cage (50 μg protein) tail injected into immunized mice at 1 and 24 hours post injection.

Table 2 Percent of injected dose/gm of tissue; t-test results

	Cages											
Tissue (Mean ± SEM)	**HspG41C (n = 7 for naïve 24 hr mice; n = 8 for immunized mice; Salivary gland n = 4 for naïve 1 and 24 hr mice)**						**CCMV K42R (n = 8)**					
	1 hr			**24 hr**			**1 hr**			**24 hr**		
	Naïve	Immunized	p-value	Naïve	Immunized	p-value	Naïve	Immunized	p-value	Naïve	Immunized	p-value
Liver	20.56 ± 3.89	45.73 ± 4.45	0.0008	0.59 ± 0.07	1.05 ± 0.17	0.03	22.79 ± 2.63	36.81 ± 1.8	0.0006	5.07 ± 0.48	3.94 ± 0.17	0.05
Spleen	15.02 ± 2.37	13.95 ± 3.05	0.79	1.12 ± 0.33	0.99 ± 0.08	0.68	14.5 ± 1.65	10.11 ± 1.28	0.05	2.45 ± 0.28	1.49 ± 0.1	0.006
Thyroid	132.6 ± 26.99	37.52 ± 11.62	0.006	483.0 ± 184.7	76.39 ± 17.13	0.04	193.0 ± 58.52	8.66 ± 1.09	0.02	126.4 ± 25.63	81.61 ± 16.4	0.16
Lung	5.09 ± 0.41	30.78 ± 6.1	0.0009	0.13 ± 0.02	0.24 ± 0.03	0.008	4.76 ± 0.62	6.82 ± 0.42	0.02	0.37 ± 0.15	0.15 ± 0.01	0.16
Kidney	7.34 ± 0.79	4.43 ± 0.5	0.007	0.19 ± 0.01	1.79 ± 0.01	0.18	9.61 ± 1.15	6.21 ± 0.25	0.01	1.44 ± 0.14	0.43 ± 0.01	<0.0001
Salivary Gland	22.04 ± 2.96	16.89 ± 4.01	0.42	0.14 ± 0.05	0.17 ± 0.02	0.58	12.36 ± 1.89	11.88 ± 0.77	0.82	0.28 ± 0.04	0.12 ± 0.02	0.004
Feces and Urine	% of dose			66.28 ± 2.3	56.63 ± 2.2	0.09				63.31 ± 3.5	59.26 ± 2.3	0.09

	p – values			
	1 hr		**24 hr**	
Tissue	Hsp Naive vs CCMV Naive[a]	Hsp Immunized vs CCMV Immunized[b]	Hsp Naive vs CCMV Naive[c]	Hsp Immunized vs CCMV Immunized[d]
Spleen	0.86	0.26	0.008	0.002
Liver	0.64	0.08	<0.0001	<0.0001
Thyroid	0.36	0.03	0.06	0.83
Lung	0.67	0.002	0.16	0.02
Kidney	0.13	0.007	<0.0001	<0.0001
Salivary Gland	0.02	0.24	0.08	0.09
Urine and Feces[e]			0.09	0.09

[a]Comparison of HspG41C naïve vs CCMV K42R naïve mice tissue at 1 hour.
[b]Comparison of HspG41C immunized vs CCMV K42R immunized mice tissue at 1 hour.
[c]Comparison of HspG41C naïve vs CCMV K42R naïve mice tissue at 24 hour.
[d]Comparison of HspG41C immunized vs CCMV K42R immunized mice tissue at 24 hour.
[e]Urine and Feces were analyzed as percentage of injected dose.

the ^{125}I-labeled cages, including hypopnea, ruffled fur, and lethargy. Signs of recovery began approximately 1.5 hrs post injection and a full recovery was apparent at 2.5 hrs post IV administration. Also, the spleens of the 1 hr CCMV injected mice were darker in color, the lungs appeared congested, and it was difficult to obtain the usual 70 μL volume of blood sample from the mice after clipping the abdominal aorta.

Immunized mice injected with either HspG41C or CCMV nanoparticles under the same conditions as the ^{125}I-injected mice did not have any remarkable histological pathology, based on observation of liver, kidney or spleen hematoxylin and eosin stained sections. However, observations of lung sections from CCMV-immunized mice revealed pulmonary vascular congestion, which may have accounted for some of the respiratory distress observed in these mice. Spleen sections from HspG41C- or CCMV-injected mice appeared different from each other; areas of white pulp in the HspG41C-injected mouse spleen were greater in size with well defined germinal centers. Serum samples taken from immunized mice prior to challenge with IV cage injections were analyzed using an ELISA technique for cage specific IgE levels; no IgE was detected (data not shown).

Discussion

These biodistribution studies demonstrated that two different protein cage based nanoparticles rapidly translocate extensively and easily throughout mouse tissues after intravenous instillation. Fluorescently labeled-HspG41C and CCMV

were found in various tissues at different time points as evidenced by epifluorescence microscopy. The particles were visibly associated with the circulatory and lymphatic endothelium, pulmonary epithelial surfaces, the interstitium of the lung, the outer capsule and perilymphoid zones of the spleen (Supplemental Figure 2), the sinusoids of the liver, the convoluted tubules of the kidney, and draining lymph nodes (Supplemental Figure 3). These results indicate the ability of these two different protein-based nanoparticles to extravasate from the vascular system to interstitial areas,

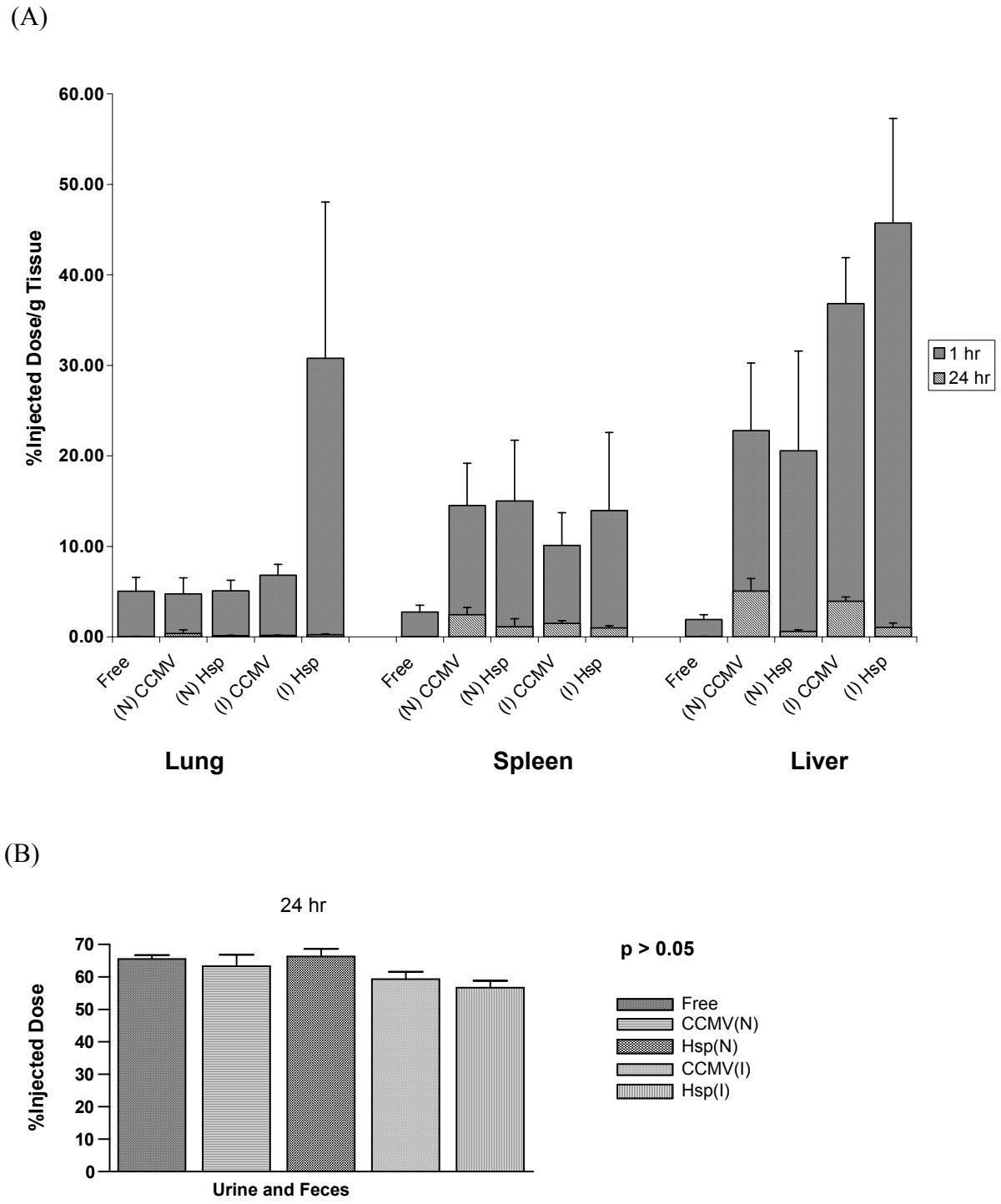

Figure 5 Comparison of selected organs from mice receiving IV free ^{125}I versus mice receiving either ^{125}I-CCMV or ^{125}I-HspG41C cage. (**A**) Percent of dose/g of lung, spleen and liver tissue at 1 and 24 hours. Naïve (N), immunized (I), and free ^{125}I (Free). (**B**) Percent of dose excreted in the urine and feces together at 24 hours.

enter into the lymphatics, possibly return to the circulatory system and again appear in interstitial areas of several organs. In this regard, fluorescently-labeled protein cages given intratracheally quickly traversed the airway epithelium, entered the lymphatics of the pulmonary interstitium and could be seen in the subcapsular sinus of the lung-associated lymph nodes within 15 minutes (data not shown).

The ^{125}I biodistribution data also indicated that both types of protein cage nanoparticles rapidly disperse throughout the mouse system freely and are not preferentially distributed to any particular tissue or organ type. Both types of cages were found at similar levels in all tissues and organs tested, except the brain. Both the ^{125}I-HspG41C and ^{125}I-CCMV disseminated in naïve mice in a similar fashion after IV injection. This is notable when considering the complete differences in amino acid composition, subunit structure and architectures and source of the nanocages. Although protein cage size differs (12 nm Hsp versus 28 nm CCMV), perhaps this is not substantial enough to influence cage distribution in mice. In spite of the differences, the two protein cages are similar in exterior charge (negative at pH 7.4) and hydrophilicity. Surprisingly, iodinated cages injected into mice previously immunized to the cages distributed in a similar pattern as that observed in naïve mice. The ability of these nanocages to distribute widely is highlighted by studies using different routes of administration. In separate trials (data not shown), 50 μg iodinated HspG41C was instilled into mice intranasally and organs taken at 1 and 24 hours. In the lungs of the 1 hour mice 5.3% ID was recovered, which differs, but not greatly, from the IV instilled mice (0.8%–1.4% ID). The pulmonary architecture is such that numerous surface areas facilitate adherence of inhaled particulate; so it is surprising that a greater deposit of nanocage is not seen considering that one dose was instilled directly into the lungs and the other intravenously. A nanoparticle drug delivery system with the ability to move rapidly throughout several tissue types may lend to the quick arrival of a therapeutic dose to a site not easily accessed by conventional medicinal delivery systems.

The high percentage of nanoparticles excreted at 24 hours (57%–73% ID) for both cage types in naïve and immunized mice is striking. The percentage of cage excreted did not significantly differ ($p = 0.09$) among the naïve versus the immunized mice. The filtration system of the kidney is such that large molecules encounter barriers of size, electrical charge, and molecular configuration before they are excreted. Normally, transport of molecules through this system excludes highly negatively charged particles and/or molecules with greater than 68,000 MW (Young et al 2006). This suggests the both the CCMV and the Hsp protein cages are being degraded prior to excretion in the urine. Further experimentation is required to determine the nature, mechanism(s), and consequence of potential release of therapeutic agents from the interior of the protein caused by possible protein cage degradation in vivo. Ultimately, genetic and chemical modification of protein cage architectures may be necessary to tailor the degradation characteristics of a particular protein cage nanostructure for optimal medical applications.

The % ID in the feces ranged from 5.9% to 7.3% and warrants consideration of hepatic circulation and bile composition. Bile produced by the parenchymal cells of the liver is composed of conjugated bile salts, phospholipids, cholesterol, and soluble proteins transcytosed across the hepatocyte from the plasma to the bile (Crawford 1996). Cholangiocytes, the epithelial cells that line the bile duct, secrete and transport proteins from the plasma into the bile; ie, sugar, amino acids, IgA, and other cytokines (Prall and LaRusso 1999). It is feasible that the iodinated protein cages may have crossed into the bile that was secreted into the upper duodenum then passed through the colon and were eliminated in the feces. Another plausible explanation is that the ^{125}I-labeled nanocages traversed across the airway mucosa, moved up the muco-ciliary escalator, and were swallowed by the mouse and transmitted through the digestive system. In this regard, capsids injected IV into mice were seen within airway lumina within minutes of injection. Overall, the rapid clearance of the particles within a 24 hour period again highlights the ability of both HspG41C and CCMV to swiftly scatter throughout the whole body without overt retention in any particular organ or cell type and then readily clear via the renal and fecal routes within 24 hours with no obvious morbidity or mortality. The ability of these nanocages to quickly exit the body, especially if they can be maintained as intact protein cage architectures, could potentially lessen the detrimental side effects of dose molecules associated with delivery vehicles that did not interact with a targeted tissue or decrease excessive exposure in the body of imaging agents delivered on either of these platforms.

The lack of significant differences in biodistribution of both types of cage structures between naïve and immunized mice may be the function of nanoparticle size. Even though no organ type was highly associated with either type of protein cage deposition, the liver and spleen were among the organs with the highest %ID/g of tissue at 1 hour in both naïve and immunized mice. Often times small size particles ($<$100 nm) have decreased opsonization and slower recogni-

tion by macrophages resulting in their ability to readily evade detection and elimination by the reticuloendothelial (RES) system (Moghimi 2001; Rossin 2005). An exception to the general biodistribution pattern is the change in biodistribution in the lung and liver between naïve and immunized mice. In the naïve ^{125}I-HspG41C and ^{125}I-CCMV injected mice the %ID/g of lung tissue ranged from 4.8 to 5.1% at 1 hour. However, in the case of the immunized mice the %ID/g of lung was 30.8 and 6.8% respectively at 1 hr. As well, in HspG41C or CCMV immunized mice, the %ID/g of liver was greater at 1 hour compared to mice not previously exposed to the nanocages (122% and 62% greater, respectively). Conceivably, the elevated percent dose in the liver and lung of immunized mice was due to the rapid formation of antibody-cage complexes and trapping by the mononuclear phagocyte system (ie, RES). Moreover, previous work that examined the biodistribution of free ^{125}I determined that the iodine-tyrosine bond is susceptible to hydrolysis by diodinase enzymes that are abundant in hepatocyte microsomes (Awasthi et al 2004). Iodine is absorbed in the GI tract gastric mucosa, the ductal cells of mouse parotid glands, submandibular glands, and follicular cells of the thyroid gland via a transmembrane sodium/iodine-symporter (Josefsson et al 2002). Therefore, it is plausible that in the case of the immunized mice, antibody-cage complexing captured in the sinusoidal compartment of the liver prevented the diodinase enzyme from working effectively in the microsomal compartment of the hepatocyte. This may offer an explanation for the greater distribution of the cage in immunized mice livers and in the case of the HspG41C-immunized mice, a lesser amount of cage in the salivary gland as compared to naïve mice at 1 hour. Furthermore, possibly more antibody-complexed CCMV cage lingered in the liver and spleen of immunized mice at 24 hours than did antibody-complexed HspG41C.

Intravenous administration of CCMV and Hsp in mice did not appear to be overtly harmful. Both the CCMV and Hsp protein cage nanoparticles were immunogenic as indicated by production of a strong IgG and IgM response. However, there were no significant differences in mouse body weight or appearance between naïve or immunized mice over a 21-day period (data not shown). In both naïve and immunized mice there was not a drastically altered biodistribution or excretion pattern of either the ^{125}I-HspG41C or ^{125}I-CCMV particles. However, IV administration of ^{125}I-HspG41C or ^{125}I-CCMV injected mice into immunized mice did produce temporary adverse responses, which are not uncommon in IV-administered therapeutics (Allen and Cullis 2004). However, like QDs and other protein-based therapeutic agents, problematical side effects might very well be overcome by protein cage modifications such as covalently linking polyethylene glycol (PEG) chains to exterior surface. Clearly, complete toxicology studies need to be performed to fully asses the mammalian biocompatibility of protein cage based therapeutic platforms.

Our results differ from those analyzing the biodistribution, circulation half-life and in vivo compatibility of fluorescently labeled Cowpea mottle viruses (CPMV) (Rae et al 2005; Lewis et al 2006). Compared to the results described herein utilizing CCMV, CPMV distributed in relatively higher amounts in the spleen, lymph nodes, kidney, liver and intestinal tract of the mice at day 1 post injection and in some cases increased in deposition in the organs over time (24 and 72 hours post injection). In contrast, both the CCMV and Hsp protein cage architectures were nearly completely eliminated from animals by 24 hours post injection. The CPMV particles were found in the parenchyma of the brain in mice receiving particles via the oral and intravenous routes (Rae et al 2005), yet in our studies the distribution of CCMV in the brain was not detected. Chick chorioallantoic membrane modeling has been used to demonstrate the usefulness of CPMV delivered fluorescent imaging dyes and it was found that CPMV localized to vascular endothelium (Lewis et al 2006). The ^{125}I-CCMV results from this study indicated that our nanoparticles were associated with vascular endothelium as well as localized interstitially, which is speculated to be the results of nonprofessional phagocytes such as liver and pulmonary endothelial cells (Steffan et al 1986; Dini et al 1995; Chen et al 2006) that engulfed the ^{125}I-CCMV. The CCMV and CPMV are similar in that both are ~28 nm particles with T = 3 icosahedral symmetry, they both have similar eight stranded β-barrel folds of the coat protein subunits that comprise the protein shell of their virus particle, and they can both systemically infect similar host plants. However, there is little amino acid similarity between the CCMV and CPMV coat proteins which may contribute to the observed biodistribution differences between the two nanoparticles. In addition, differences in particle structure may also alter how each type of particle interacts in mice. The observed differences between CCMV and CPMV nanoparticles reinforces the notion that it is difficult to predict how seemingly very similar nanopartices will behave in vivo.

There are many parallels and differences between the biodistribution characteristics of viral and non-viral protein based nanoparticles and QDs. In general, IV administration of both types of nanoparticles results in broad tissue and organ

distribution within tested animals. Both are not overtly toxic to animals and surface modifications (eg, pegylation) (Owens and Peppas 2006) can be used to tailor their biocompatibility properties for applications in medicine. In contrast to QDs, the protein cage nanoplatforms examined here did not preferentially accumulate and persist within mice tissues and organs (especially the liver), providing a potential benefit as therapeutic and imaging agents. However, in comparison to QDs, both the CCMV and Hsp protein cages are likely more immunogenic, indicating that immunological response to each type of protein cage platform will have to be fully addressed and tailored before they will find broad application in medicine.

This work contributes fundamental baseline information on the biocompatibility of protein cage nanoplatforms. The broad distribution and movement through tissues, the rapid excretion, and a lack of preferential distribution may render possible advantages for the use of Hsp or CCMV as safe, biocompatible, nanoplatforms for applications in medicine and support the need for further in vivo investigation into the application of protein based nanocages as therapeutic and imaging platforms.

Acknowledgments

The authors would like to thank Debbie Willits, Diana Buckner, Ann Willis and Susan Brumfield for their assistance and Drs. Steven Swain, Martin Teintze, and Mark Quinn for critical reading of the manuscript.

References

Allen M, Willits D, Mosolf J, et al. 2002. Protein cage constrained synthesis of ferrimagnetic iron oxide nanoparticles. *Advanced Materials*, 14:1562.

Allen MA, Leipold LO, Bulte JWM, et al. 2005. Paramagnetic viral nanoparticles as potential high-relaxivity MRI contrast agents. *Magn Reson Med*, 54:807–12.

Allen TM, Cullis PR. 2004. Drug delivery systems: entering the mainstream. *Science*, 303:1818–22.

Awasthi V, Meinken G, Springer K, et al. 2004. Biodistribution of radioiodinated adenovirus fiber protein knob domain after intravenous injection in mice. *J Virol*, 78:6431–8.

Bancroft JB, Hiebert E. 1967. Formation of an infectious nucleoprotein from protein and nucleic acid isolated from a small spherical virus. *Virology*, 32:354–6.

Barratt G. 2003. Colloidal drug carriers: achievements and perspectives. *Cell Mol Life Sci*, 60:21–37.

Blum AS, Soto CM, Wilson CD, et al. 2004. Cowpea mosaic virus as a scaffold for 3-D patterning of gold nanoparticles. *Nano Letters*, 4:867–70.

Brennan FR, Jones TD, Hamilton WD. 2001. Cowpea mosaic virus as a vaccine carrier of heterologous antigens. *Mol Biotechnol*, 17:15–26.

Brigger I, Dubernet C, Couvreur P. 2002. Nanoparticles in cancer therapy and diagnosis. *Adv Drug Deliv Rev*, 54:631–51.

Bruchez M Jr, Moronne M, Gin P, et al. 1998. Semiconductor nanocrystals as fluorescent biological labels. *Science*, 281:2013–6.

Brumfield S, Willits D, Tang L, et al. 2004. Heterologous expression of modified Cowpea chlorotic mottle bromovirus coat protein results in the assembly of protein cages with altered architectures and function. *Journal of General Virology*, 85:1049–53.

Chatterji A, Burns LL, Taylor SS, et al. 2002. Cowpea mosaic virus: from the presentation of antigenic peptides to the display of active biomaterials. *Intervirology*, 45:362–70.

Chen Q, Stone PR, McCowan LM, et al. 2006. Phagocytosis of necrotic but not apoptotic trophoblasts induces endothelial cell activation. *Hypertension*, 47:116–21.

Choi Y, Thomas T, Kotlyar A, et al. 2005. Synthesis and functional evaluation of DNA-assembled polyamidoamine dendrimer clusters for cancer cell-specific targeting. *Chem Biol*, 12:35–43.

Crawford JM. 1996. Role of vesicle-mediated transport pathways in hepatocellular bile secretion. *Semin Liver Dis*, 16:169–89.

Damge C, Michel C, Aprahamian M, et al. 1988. New approach for oral administration of insulin with polyalkylcyanoacrylate nanocapsules as drug carrier. *Diabetes*, 37:246–51.

Dini L, Lentini A, Diez GD, et al. 1995. Phagocytosis of apoptotic bodies by liver endothelial cells. *J Cell Sci*, 108(Pt 3):967–73.

Douglas T, Young M. 1998. Host-guest encapsulation of materials by assembled virus protein cages. *Nature* (*London*), 393:152–5.

Emerich DF, Thanos CG. 2003. Nanotechnology and medicine. *Expert Opin Biol Ther*, 3:655–63.

Flenniken M, Young M, Douglas T. 2004. Viruses as host assemblies. In: Steed W, Atwood JL ed. Encyclopedia of supramolecular chemistry. New York City: Marcel Dekker, Inc. p 1563–8.

Flenniken ML, Liepold LO, Crowley BE, et al. 2005. Selective attachment and release of a chemotherapeutic agent from the interior of a protein cage architecture. *Chem Commun (Camb)*, 28:447–9.

Flenniken ML, Willits DA, Brumfield S, et al. 2003. The small heat shock protein cage from Methanococcus jannaschii is a versatile nanoscale platform for genetic and chemical modification. *NanoLetters*, 3:1573–6.

Flenniken ML, Willits DA, Harmsen AL, et al. 2006. Melanoma and lymphocyte cell-specific targeting incorporated into a heat shock protein cage architecture. *Chem Biol*, 13:161–70.

Fox JM, Zhao X, Speir JA, et al. 1996. Analysis of a salt stable mutant of cowpea chlorotic mottle virus. *Virology*, 222:115–22.

Francki RIB. 1985. The viruses and their taxonomy. In: The plant viruses. New York, NY: Plenum Press.

Fundaro A, Cavalli R, Bargoni A, et al. 2000. Non-stealth and stealth solid lipid nanoparticles (SLN) carrying doxorubicin: pharmacokinetics and tissue distribution after i.v. administration to rats. *Pharmacol Res*, 42:337–43.

Gillitzer E, Suci P, Young M, et al. 2006. Controlled ligand display on a symmetrical protein cage architecture through mixed assembly. *Small*, in press.

Gillitzer E, Willits D, Young M, et al. 2002. Chemical modification of a viral cage for multivalent presentation. *Chem Commun (Camb)*, 21:2390–1.

Gurdag S, Khandare J, Stapels S, et al. 2006. Activity of dendrimer-methotrexate conjugates on methotrexate-sensitive and resistant cell lines. *Bioconjug Chem*, 17:275–83.

Hardman R. 2006. A toxicologic review of quantum dots: toxicity depends on physicochemical and environmental factors. *Environ Health Perspect*, 114:165–72.

Hooker JM, Kovacs EW, Francis MB. 2004. Interior surface modification of bacteriophage MS2. *J Am Chem Soc*, 126:3718–9.

Jana SS, Bharali DJ, Mani P, et al. 2002. Targeted cytosolic delivery of hydrogel nanoparticles into HepG2 cells through engineered Sendai viral envelopes. *FEBS Lett*, 515:184–8.

Janes KA, Calvo P, Alonso MJ. 2001. Polysaccharide colloidal particles as delivery systems for macromolecules. *Adv Drug Deliv Rev*, 47:83–97.

Josefsson M, Grunditz T, Ohlsson T, et al. 2002. Sodium/iodide-symporter: distribution in different mammals and role in entero-thyroid circulation of iodide. *Acta Physiol Scand*, 175:129–37.

Kayser O, Lemke A, Hernandez-Trejo N. 2005. The impact of nanobiotechnology on the development of new drug delivery systems. *Current Pharmaceutical Biotechnology*, 6:3–5.

Kim KK, Kim R, Kim SH. 1998a. Crystal structure of a small heat-shock protein. *Nature*, 394:595–9.

Kim R, Kim KK, Yokota H, et al. 1998b. Small heat shock protein of Methanococcus jannaschii, a hyperthermophile. *Proc Natl Acad Sci USA*, 95:9129–33.

Lee RJ, Low PS. 1995. Folate-mediated tumor cell targeting of liposome-entrapped doxorubicin in vitro. *Biochim Biophys Acta*, 1233:134–44.

Lewis JD, Destito G, Zijlstra A, et al. 2006. Viral nanoparticles as tools for intravital vascular imaging. *Nat Med*, 12:354–60.

Loo C, Hirsch L, Lee MH, et al. 2005. Gold nanoshell bioconjugates for molecular imaging in living cells. *Opt Lett*, 30:1012–4.

Loo C, Lin A, Hirsch L, et al. 2004. Nanoshell-enabled photonics-based imaging and therapy of cancer. *Technol Cancer Res Treat*, 3:33–40.

Moghimi S, Hunter AC, Murray JC. 2001. Long-circulating and target-specific nanoparticles: theory to practice. *Pharmacological reviews*, 53:283–318.

Moghimi SM, Hunter AC, Murray JC. 2005. Nanomedicine: current status and future prospects. *Faseb J*, 19(3):311–30.

Muller K, Nahde T, Fahr A, et al. 2001. Highly efficient transduction of endothelial cells by targeted artificial virus-like particles. *Cancer Gene Ther*, 8:107–17.

Na K, Bae YH. 2002. Self-assembled hydrogel nanoparticles responsive to tumor extracellular pH from pullulan derivative/sulfonamide conjugate: characterization, aggregation, and adriamycin release in vitro. *Pharm Res*, 19:681–8.

Nel A, Xia T, Madler L, et al. 2006. Toxic potential of materials at the nanolevel. *Science*, 311:622–7.

Owens DE 3rd, Peppas NA. 2006. Opsonization, biodistribution, and pharmacokinetics of polymeric nanoparticles. *Int J Pharm*, 307:93–102.

Powers KW, Brown SC, Krishna VB, et al. 2006. Research strategies for safety evaluation of nanomaterials. Part VI. Characterization of nanoscale particles for toxicological evaluation. *Toxicol Sci*, 90:296–303.

Prall RT, LaRusso NF. 1999. Biliary tract physiology. *Current Opinion in Gastroenterology*, 15(5):423–29.

Rae CS, Khor IW, Wang Q, et al. 2005. Systemic trafficking of plant virus nanoparticles in mice via the oral route. *Virology*, 343:224–35.

Raja KS, Wang Q, Gonzalez MJ, et al. 2003. Hybrid virus-polymer materials. 1. Synthesis and properties of PEG-decorated cowpea mosaic virus. *Biomacromolecules*, 4:472–6.

Ramsay B, Wiedenheft B, Allen M, et al. 2006. Dps-like protein from the hyperthermophilic archaeon Pyrococcus furiosus. *Journal of Inorganic Biochemistry*, 100:1061–8.

Rossin R, Pan D, Qi K, et al. 2005. ^{64}Cu-labeled folate-conjugated shell cross-linked nanoparticles for tumor imaging and radiotherapy: synthesis, radiolabeling, and biologic evaluation. *J Nucl Med*, 46:1210–8.

Roy I, Ohulchanskyy TY, Pudavar HE, et al. 2003. Ceramic-based nanoparticles entrapping water-insoluble photosensitizing anticancer drugs: a novel drug-carrier system for photodynamic therapy. *J Am Chem Soc*, 125:7860–5.

Service RF. 2005a. Materials and biology. Nanotechnology takes aim at cancer. *Science*, 310:1132–4.

Service RF. 2005b. Nanotechnology. Calls rise for more research on toxicology of nanomaterials. *Science*, 310:1609.

Singh P, Destito G, Schneemann A, et al. 2006. Canine parvovirus-like particles, a novel nanomaterial for tumor targeting. *J Nanobiotechnology*, 4:2.

Speir JA, Munshi S, Baker TS, et al. 1993. Preliminary x-ray data analysis of crystalline cowpea chlorotic mottle virus. *Virology*, 193:234–41.

Speir JA, Munshi S, Wang G, et al. 1995. Structures of the native and swollen forms of cowpea chlorotic mottle virus determined by x-ray crystallography and cryo-electron microscopy. *Structure*, 3:63–78.

Steffan AM, Gendrault JL, McCuskey RS, et al. 1986. Phagocytosis, an unrecognized property of murine endothelial liver cells. *Hepatology*, 6:830–6.

Sun X, Rossin R, Turner JL, et al. 2005. An assessment of the effects of shell cross-linked nanoparticle size, core composition, and surface PEGylation on in vivo biodistribution. *Biomacromolecules*, 6:2541–54.

Wickline SA, Lanza GM. 2003. Nanotechnology for molecular imaging and targeted therapy. *Circulation*, 107:1092–5.

Wiedenheft B, Mosolf J, Willits D, et al. 2005. An archaeal antioxidant: characterization of a Dps-like protein from Sulfolobus solfataricus. *Proc Natl Acad Sci USA*, 102:10551–6.

Yoo HS, Lee KH, Oh JE, et al. 2000. In vitro and in vivo anti-tumor activities of nanoparticles based on doxorubicin-PLGA conjugates. *J Control Release*, 68:419–31.

Yoo HS, Oh JE, Lee KH, et al. 1999. Biodegradable nanoparticles containing doxorubicin-PLGA conjugate for sustained release. *Pharm Res*, 16:1114–8.

Young B, Lowe JS, Stevens A, et al. 2006. Wheater's functional histology a text and colour atlas. Churchill Livingstone Elsevier.

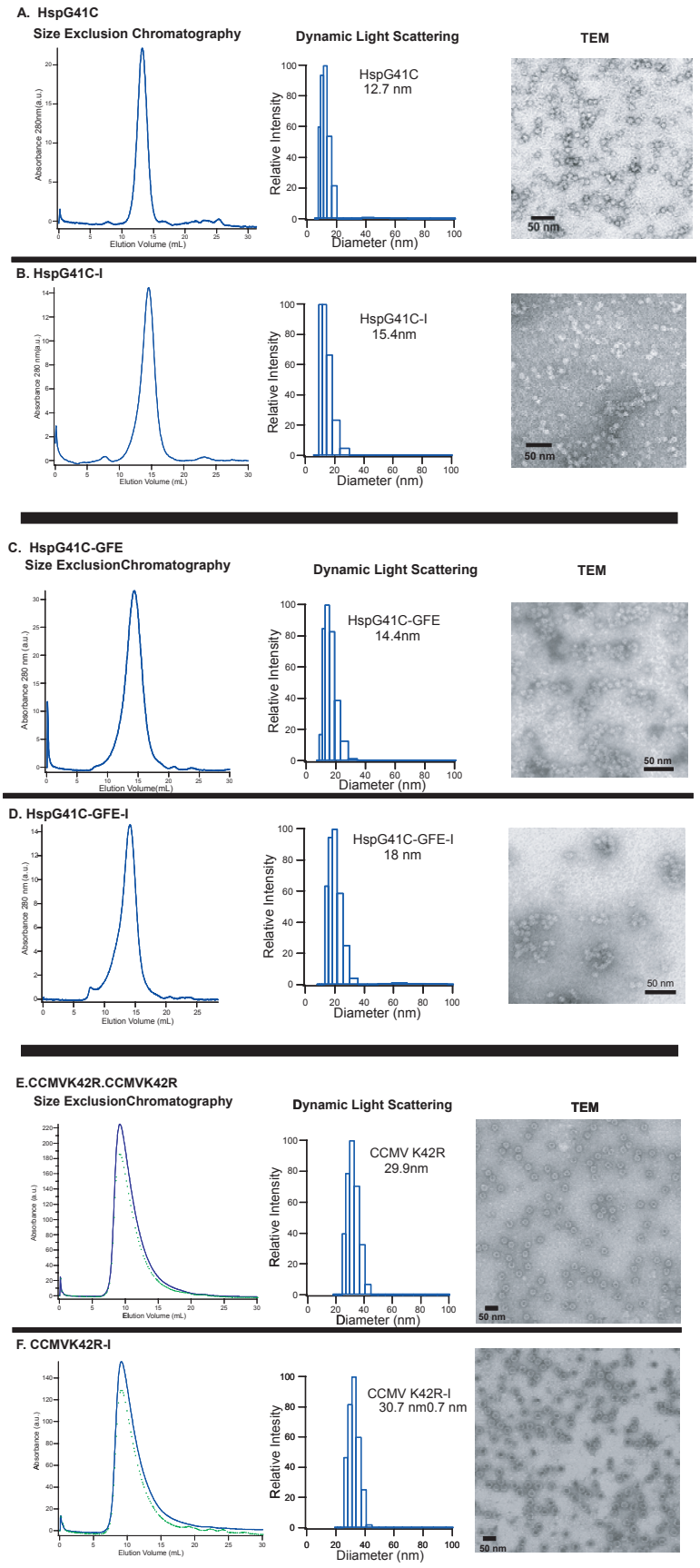

Supplemental Figure 1 Characterizations of HspG41C, HspG41C-GFE, and CCMV K42R Before (**A**, **C**, **E**) and After (**B**, **D**, **F**) Iodination.

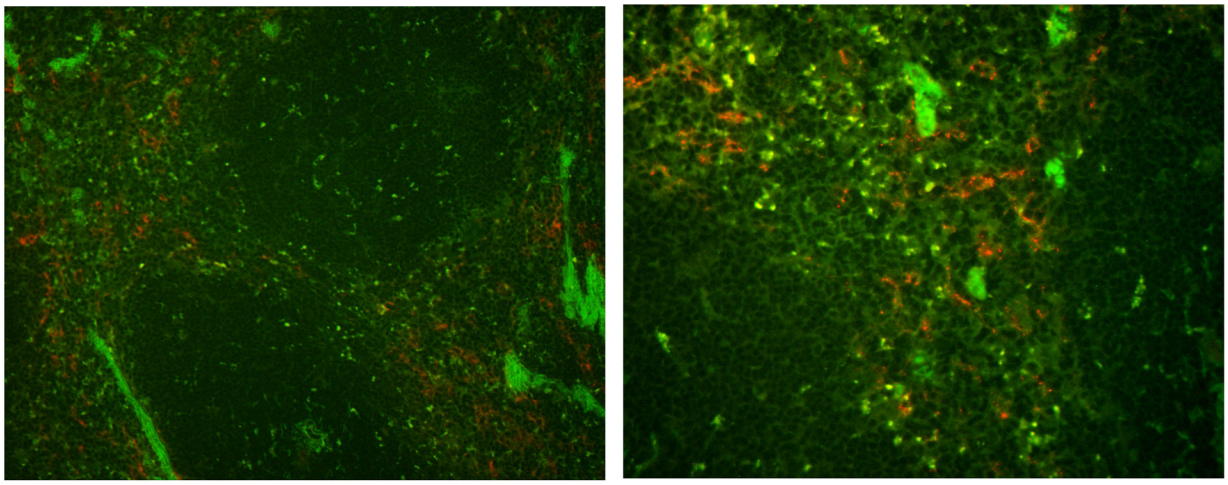

Supplemental Figure 2 Epifluorescence microscopy displaying Texas Red-labeled HspG41C cage in mouse spleen at 30 minutes post IV instillation of 105 μg protein. (**a**) Transverse cryostat spleen section; labeled particles appear in the red pulp surrounding the periarterial lymphoid sheaths (200x original magnification). (**b**) Same tissue at higher magnification (400x original).

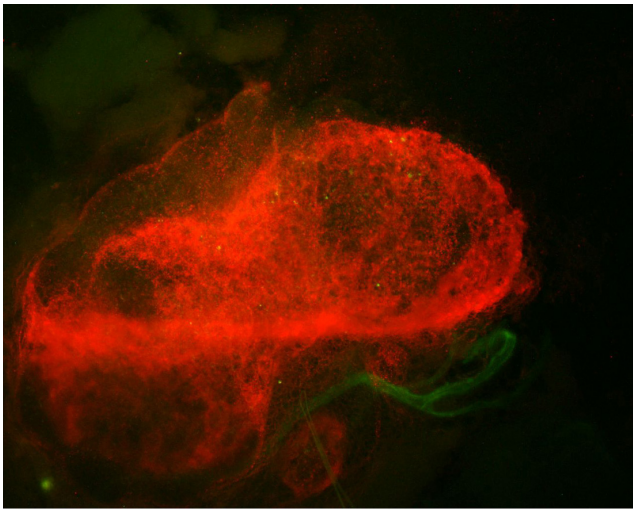

Supplemental Figure 3 Fluorescently labeled HspG41C particles identified in lung-associated lymph nodes. Epifluorescence microscopy views of a tracheobronchial lymph node excised from a mouse at 3 hours after IV instillation of 50 μg Texas Red-HspG41C (40x original magnification).